

Optimizing superlattice bilayer graphene for a fractional Chern insulator

Dathan Ault-McCoy,¹ M. Nabil Y. Lhachemi,¹ Aaron Dunbrack,^{2,1} Sayed Ali Akbar Ghorashi,¹ and Jennifer Cano^{1,3}

¹*Department of Physics and Astronomy, Stony Brook University, Stony Brook, New York 11794, USA*

²*Department of Physics and Nanoscience Center, University of Jyväskylä,*

P.O. Box 35, FI-40014 University of Jyväskylä, Finland

³*Center for Computational Quantum Physics, Flatiron Institute, New York, New York 10010, USA*

(Dated: May 12, 2025)

Bernal-stacked bilayer graphene modulated by a superlattice potential is a highly tunable system predicted to realize isolated topological flat bands. In this work we calculate the band structure and quantum geometry of bilayer graphene subject to both triangular and square superlattices, across a wide range of gate voltages. We identify the parameter regime that optimizes the “single-particle indicators” for the stability of a fractional Chern insulator (FCI) when a topological flat band is partially filled. Our results guide the experimental realization of an FCI in this platform.

I. INTRODUCTION

The discovery of superconductivity and correlated insulators in twisted bilayer graphene (TBG) launched the field of moiré materials [1–4]. Moiré materials generically exhibit flat bands as a consequence of an emergent, nanometer-scale moiré superlattice. Often, these flat bands inherit topology from their constituent layers [5–11], which is responsible for the observation of the anomalous Hall effect in both TBG [12, 13] and twisted transition metal dichalcogenide (TMD) heterobilayers [14]. In a finite magnetic field, Chern insulators – lattice-analogs of quantum Hall states – have also been observed in TBG [15, 16], building on earlier observations in graphene heterostructures aligned with hexagonal boron nitride (hBN) [17–20].

Despite these observations, the long sought-after zero-field fractional Chern insulator (FCI) [21–23] has remained elusive in TBG. Instead, the first observation of a zero-field FCI appeared recently in twisted MoTe₂ [24–26]. The second observation followed shortly after in rhombohedral graphene aligned with hBN [27, 28]. These two observations in diverse experimental platforms give optimism that more realizations will soon follow.

Recently, experimental advances in gate-patterning [29–35] and moiré [36–41] and molecular engineering [42] have inspired an increasingly diverse array of proposals for new systems with designer superlattice geometry beyond the twisted bilayers [43–49]. In this paper, we study one such system which has been put forward as a promising platform to realize an FCI [44, 49]: Bernal-stacked bilayer graphene subject to a spatially periodic electric potential, henceforth referred to as superlattice bilayer graphene (sBLG). This system can be realized by the experimental setup depicted in Fig. 1, where the superlattice potential is defined by a patterned electrode. This platform may avoid some practical challenges of moiré heterostructures [50], while offering independent control over the superlattice geometry, length scale, and potential strength, the last of which is tunable *in situ*.

While experimental evidence for correlated phenomena in sBLG has been observed and attributed

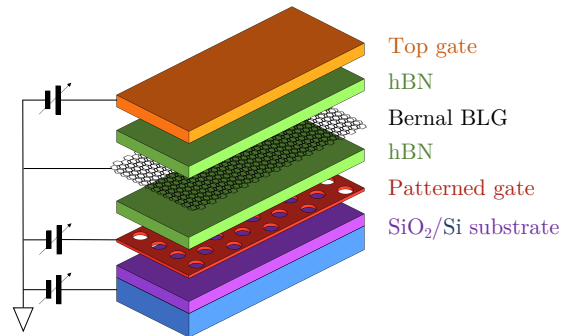


FIG. 1. Schematic of an experimental set-up realizing sBLG. A spatially modulated electric potential is generated on Bernal-stacked bilayer graphene by a nanopatterned bottom gate. Along with uniform top and bottom gates, the spatially modulated potential, spatially constant displacement field and the electron density can all be independently tuned.

to superlattice-induced flat bands [34], the theoretically predicted topological regime has not been realized. The purpose of the present work is to systematically characterize the parameter space of sBLG and determine the optimal parameters to realize an FCI. As a proxy for FCI stability, we employ single-particle indicators based on quantum band geometry, which we will describe shortly. Our work serves as a guide for future experimental studies of this platform.

II. MODEL

We model the band structure of sBLG by the Hamiltonian

$$H = H_{\text{BLG}} + H_V. \quad (1)$$

The first term describes an effective continuum model for bilayer graphene derived by expanding a tight binding model around the K or K' high-symmetry point [51], and is given by $H_{\text{BLG}} = \sum_{\mathbf{k}} c_{\mathbf{k}}^{\dagger} \mathcal{H}_{\text{BLG}}(k) c_{\mathbf{k}}$,

where $c_{\mathbf{k}} = (c_{\mathbf{k},A1} \ c_{\mathbf{k},B1} \ c_{\mathbf{k},A2} \ c_{\mathbf{k},B2})^T$, the operator $c_{\mathbf{k},Ij}$ annihilates an electron with quasimomentum \mathbf{k} on sublattice I and layer j (with $j = 1$ corresponding to the top layer in Fig. 1), and

$$\mathcal{H}_{BLG}(k) = \begin{pmatrix} 0 & vk^* & -v_4 k^* & v_3 k \\ vk & 0 & t & -v_4 k^* \\ -v_4 k & t & 0 & v_3 k^* \\ v_3 k^* & -v_4 k & vk & 0 \end{pmatrix}. \quad (2)$$

Here, $k = k_x + i\chi k_y$ is the complexified quasimomentum with $\chi \in \{+, -\}$ the valley index. In the remainder of this work, we will specialize to the K valley, taking $\chi = +$. In Eq. (2), v is the Fermi velocity, t is the nearest-neighbor inter-layer hopping strength, and v_3 and v_4 arise from next-to-nearest-neighbor hopping contributions. These latter two terms result in trigonal warping of the Fermi surface and electron-hole asymmetry, respectively. Though they were omitted in previous work, e.g., Ref. [44], for the purposes of the present work, we find their effects quantitatively significant enough to warrant inclusion.

The electric potential applied to the sample is included through

$$H_V = \int d\mathbf{r} \sum_{I,j} \psi_{Ij}^\dagger(\mathbf{r}) \psi_{Ij}(\mathbf{r}) [(-1)^j V_0 + \alpha_j V_{SL}(\mathbf{r})], \quad (3)$$

where $\psi_{Ij}(\mathbf{r}) = \sum_{\mathbf{k}} c_{\mathbf{k},Ij} e^{i\mathbf{k}\cdot\mathbf{r}}$, V_0 is a uniform interlayer displacement potential, and $V_{SL}(\mathbf{r})$ is the spatially modulated part of the potential. The symbol α_j is introduced to capture the screening effect of the second graphene layer on the potential felt by the first, and is defined by $\alpha_1 = \alpha$ and $\alpha_2 = 1$, where $\alpha \leq 1$ is a parameter of the model. We further assume that $V_{SL}(\mathbf{r})$ is simple harmonic and so can be written as

$$V_{SL}(\mathbf{r}) = V_{SL} \sum_n \cos(\mathbf{Q}_n \cdot \mathbf{r}), \quad (4)$$

where the \mathbf{Q}_n are a subset of the reciprocal vectors of the superlattice. In this work we will only consider triangular and square superlattice geometries, for which we take $\mathbf{Q}_n = 4\pi/\sqrt{3}L(\cos(2\pi n/6), \sin(2\pi n/6))$, $n = 0, \dots, 5$ and $\mathbf{Q}_n = 2\pi/L(\cos(2\pi n/4), \sin(2\pi n/4))$, $n = 0, \dots, 3$, respectively. L defines the superlattice periodicity. Note also that in the experimental setup depicted in Fig. 1, V_{SL} and V_0 can be tuned independently by varying the voltages on the unpatterned (top) and patterned (bottom) electrodes.

To summarize, the model has eight numerical parameters. For the hopping parameters in \mathcal{H}_{BLG} , we use values of $t = 380$ meV, $v = 673$ meV nm, $v_3 = 81$ meV nm and $v_4 = 30$ meV nm, as determined by infrared spectroscopy [52]. The screening constant α is determined by both the material properties of graphene and the gate design, and is taken to be 0.3 based on Ref. [53]. That leaves L , V_{SL} , and V_0 as the tunable parameters. For the analysis presented in Sec. IV, we

fix $L = 30$ nm and scan the remaining parameter space spanned by V_{SL} and V_0 . In Sec. V we briefly discuss how the results vary with L .

III. SINGLE-PARTICLE FCI INDICATORS

A Bloch band is described by its dispersion $E(\mathbf{k})$ and its quantum geometry. The latter is encoded in the quantum geometric tensor (QGT), defined as

$$G^{ab}(\mathbf{k}) = \langle D^a u_{\mathbf{k}} | D^b u_{\mathbf{k}} \rangle, \quad (5)$$

where $D^a = \partial_{\mathbf{k}}^a - iA^a(\mathbf{k})$ is the covariant derivative in momentum space, $A^a(\mathbf{k}) = -i \langle u_{\mathbf{k}} | \partial_{\mathbf{k}}^a u_{\mathbf{k}} \rangle$ is the Berry connection, and $u_{\mathbf{k}}$ is the periodic part of the Bloch wavefunction with quasimomentum \mathbf{k} . The QGT is a gauge-invariant quantity that captures how $u_{\mathbf{k}}$ varies with \mathbf{k} . Since the QGT is Hermitian, its real part, denoted $g^{ab}(\mathbf{k})$, is a symmetric form referred to as the quantum metric or the Fubini-Study metric. Its imaginary part is equal to $\frac{1}{2}\epsilon^{ab}\Omega(\mathbf{k})$, where ϵ^{ab} is the two-dimensional anti-symmetric Levi-Civita symbol and

$$\Omega(\mathbf{k}) = \partial_{\mathbf{k}}^1 A^2(\mathbf{k}) - \partial_{\mathbf{k}}^2 A^1(\mathbf{k}) \quad (6)$$

is the (scalar) Berry curvature. The Berry curvature is related to the Chern number \mathcal{C} of the band by

$$\mathcal{C} = \frac{1}{2\pi} \int_{BZ} d\mathbf{k} \Omega(\mathbf{k}), \quad (7)$$

where the integral is over the first Brillouin zone. The Chern number is always an integer; when $\mathcal{C} \neq 0$ we refer to the band as topological or a Chern band. At all values of \mathbf{k} , the quantum metric and Berry curvature obey the inequalities

$$\frac{1}{2} \text{tr } g(\mathbf{k}) \geq \sqrt{\det g(\mathbf{k})} \geq \frac{1}{2} |\Omega(\mathbf{k})|, \quad (8)$$

which follows from the positive semi-definiteness of the QGT. If the Berry curvature has the same sign everywhere in the Brillouin zone, this implies

$$\text{tr } \bar{g} \geq 2\pi|\mathcal{C}|, \quad (9)$$

where

$$\bar{g}^{ab} = \int_{BZ} d\mathbf{k} g^{ab}(\mathbf{k}) \quad (10)$$

is the integrated quantum metric.

In the presence of Coulomb interactions, a fractionally filled Chern band may realize an FCI ground state. Verifying the FCI ground state computationally requires an expensive many-body calculation. In this manuscript, following earlier literature [54–64], we predict the result of such a calculation using “single-particle indicators,” which are features of the band structure that quantify how much the Chern band resembles a lowest Landau

level (LLL). While the single-particle indicators do not guarantee an FCI ground state (and have known limitations [65]), they provide an efficient search of the large parameter space we want to study.

We now describe the single-particle indicators that we employ. By imposing a magnetic Brillouin zone, the LLL can be interpreted as a Bloch-like energy band with $|\mathcal{C}| = 1$, which is completely degenerate (i.e., $E(\mathbf{k})$ is constant), has uniform quantum geometry (i.e., $G(\mathbf{k})$ is constant), and saturates the inequality (8) [60]. Based on these properties, multiple conditions for LLL mimicry have been proposed.

The first condition is that the bandwidth

$$W = \max_{\mathbf{k}} E(\mathbf{k}) - \min_{\mathbf{k}} E(\mathbf{k}) \quad (11)$$

should be minimized so that correlation effects dominate the kinetic energy contribution.

Since the LLL has uniform Berry curvature, the second condition is that spatial variations in the Berry curvature should be minimized, i.e.,

$$F = \left[A_{\text{BZ}} \int_{\text{BZ}} d\mathbf{k} \left(\frac{\Omega(\mathbf{k})}{2\pi} - \frac{\mathcal{C}}{A_{\text{BZ}}} \right)^2 \right]^{1/2} \quad (12)$$

should be minimized, where A_{BZ} is the area of the Brillouin zone. This condition was supported by early exact diagonalization studies in a variety of lattice models [57], and it was shown that in the limit of $F = 0$, the band recovers the Girvin-Macdonald-Platzman density operator algebra of the LLL at long wavelengths [54].

More recently, the importance of the quantum metric and the inequality (8) has also been highlighted. Specifically, it has been shown that wavefunctions of “ideal” flat bands, defined as $|\mathcal{C}| = 1$ bands in which $\Omega(\mathbf{k})$ does not vanish and (8) is saturated, are proportional to LLL wavefunctions with a momentum-independent prefactor [60]. This mapping allows the construction of Laughlin-like many-body wavefunctions that are exact zero-energy eigenstates of a generalized Haldane pseudopotential Hamiltonian [60]. Models that exactly satisfy these criteria do exist, e.g., the chiral limit of twisted bilayer graphene [59], though the model we consider in this work has no such known limit. Therefore, we instead seek to minimize

$$\bar{T} = |\text{tr } \bar{g}| - 2\pi|\mathcal{C}|, \quad (13)$$

which quantifies the deviation from saturation of (8). (Note that $\bar{T} = 0$ implies that (9) is saturated, which in turn implies saturation of (8) at all \mathbf{k} .)

Although not strictly within the framework of LLL mimicry, it is also important for the band gap

$$\Delta = \min \left\{ \min_{\mathbf{k}} E_{n+1}(\mathbf{k}) - \max_{\mathbf{k}} E_n(\mathbf{k}), \min_{\mathbf{k}} E_n(\mathbf{k}) - \max_{\mathbf{k}} E_{n-1}(\mathbf{k}) \right\} \quad (14)$$

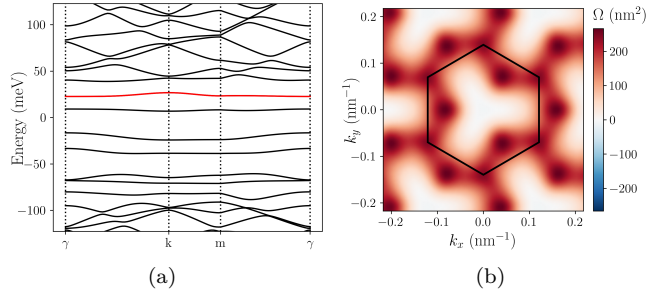


FIG. 2. (a) Band structure of triangular sBLG with $L = 30$ nm, $V_{\text{SL}} = 30$ meV, and $V_0 = -30$ meV. The $n = 0$ band is highlighted. Lowercase labels on the horizontal axis refer to the high-symmetry points of the superlattice Brillouin zone. (b) Berry curvature distribution for the $n = 0$ band, which is topological with $\mathcal{C} = +1$. The boundary of the first superlattice Brillouin zone is overlaid in black.

(where we have momentarily introduced a band index to E , with n corresponding to the band of interest) to be large compared to the interaction scale, so that the effect of neighboring bands can be ignored.

In summary, the single-particle features we seek as indicators that a band with $|\mathcal{C}| = 1$ is most suitable to host a stable FCI phase are minimal W , \bar{T} , and F , and maximal Δ .

IV. OPTIMIZING THE POTENTIAL PARAMETERS

In this section, we compute the single-particle indicators defined in Sec. III as functions of the electrically tunable parameters V_{SL} and V_0 for multiple bands in both triangular and square sBLG. The superlattice length scale is fixed at $L = 30$ nm, with discussion of other values deferred to Sec. V. The goal is to map the topological phase diagram of the system and identify the parameter regions where an FCI ground state is most likely to exist.

A. Triangular superlattice

We begin by considering a triangular superlattice geometry with $L = 30$ nm. The reciprocal lattice vectors are listed below Eq. (4). The band structure for this system is shown in Fig. 2(a) at example parameter values of $(V_{\text{SL}}, V_0) = (30 \text{ meV}, -30 \text{ meV})$. The appearance of multiple stacked, low-dispersion bands is typical. We label the bands in ascending energy order with an index n , with the $n = 0$ band highlighted in red. At $(V_{\text{SL}}, V_0) = (0, 0)$, the $n = 0$ band is the lowest band lying above the Fermi level, but at the parameter values shown it is the second lowest. Furthermore, at these parameter values, the $n = 0$ band is topological with $\mathcal{C} = +1$ (see Fig. 2(b) for the Berry curvature distribution), while

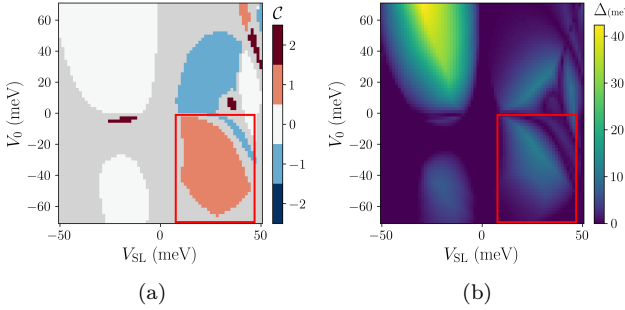


FIG. 3. (a) Chern number \mathcal{C} and (b) band gap Δ of the $n = 0$ band of $L = 30$ nm triangular sBLG. Grayed regions of (a) indicate that the Chern number is not numerically well-resolved due to the proximity of a band closing. The red box highlights the $\mathcal{C} = +1$ phase which is of primary interest for realizing an FCI. Single-particle indicators in this region are shown in Fig. 4.

the neighboring $n = 1, -1, -2$, and -3 flatbands are topologically trivial. We will ultimately find that the $n = 0$ band is topological across the widest range of parameter values and hosts the most optimal indicator values, so it is the first we will consider.

1. $n = 0$ band

Fig. 3 shows the Chern number \mathcal{C} and band gap Δ of the $n = 0$ band as functions of V_{SL} and V_0 . (Gray regions of Fig. 3(a) indicate that the Chern number is not numerically well-resolved due to the proximity of a band closing; note the coincidence of these regions with dark regions of Fig. 3, where Δ is small.) There are two prominent, approximately symmetric $|\mathcal{C}| = 1$ phases present which are of primary interest in our search for a stable FCI state. (When $\alpha = 1$, the two phases are related by an exact symmetry under PT , where P is inversion around an AB stacking point and T is time reversal. PT commutes with H_{BLG} but sends $(V_{\text{SL}}, V_0) \rightarrow (V_{\text{SL}}, -V_0)$.) The $\mathcal{C} = +1$ region with $V_0 < 0$ (indicated by the red box) has slightly more favorable indicators and so will be our focus. Other topological phases are present as well, including some with $|\mathcal{C}| > 1$; however, these phases require fine-tuning of the parameters (V_{SL}, V_0) to within a few meV and do not attain band gaps of greater than 5 meV, so we do not consider them in this work.

The single-particle indicators for FCI stability—band gap Δ , band width W , ideality deviation \bar{T} , and Berry curvature fluctuation F —are shown for the $\mathcal{C} = +1$ phase in Fig. 4. Δ is sharply maximized in a linear region of parameter space, extending from roughly $(V_{\text{SL}}, V_0) = (20 \text{ meV}, -12 \text{ meV})$ to $(35 \text{ meV}, -35 \text{ meV})$. (See the red line in Fig. 4.) F is also minimized, though less sharply, in the same region, which is consistent with the tendency for Berry curvature to accumulate in the Brillouin zone

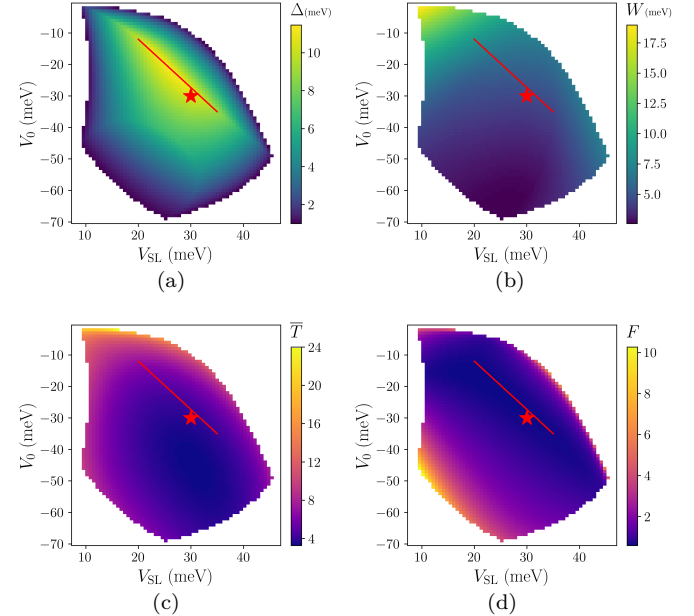


FIG. 4. Indicators (a) Δ , (b) W , (c) \bar{T} , and (d) F for the $n = 0$ band of triangular sBLG, in the $\mathcal{C} = +1$ phase highlighted in Fig. 3. The “optimal line” along which Δ and F are jointly optimized is indicated. The red star marks $(V_{\text{SL}}, V_0) = (30 \text{ meV}, -30 \text{ meV})$, the parameters used in Fig. 2, which the indicators shown here also suggest are near-optimal for realizing an FCI in this region.

	Δ (meV)	W (meV)	U_c (meV)	\bar{T}	F
sBLG	10.3	4.5	~ 5	3.8	0.63
TBG	12	11	~ 20	2-5	2-12
TBG+HF	0	30-40	~ 20	2-4	2-3
tMoTe ₂	8	6.5	~ 30	1	0.1
tMoTe ₂ +HF	35	1.2	~ 30	0.7	0.2

FIG. 5. Comparison of FCI indicators for $L = 30$ nm triangular sBLG at $(V_{\text{SL}}, V_0) = (30 \text{ meV}, -30 \text{ meV})$ in the $n = 0$ band; $\theta = 1.05^\circ$ magic-angle TBG, both with [66] and without [59, 67] Hartree-Fock (HF) corrections; and $\theta = 3.7^\circ$ twisted MoTe₂ (tMoTe₂) in the top valence band, both with and without HF corrections [68]. Values for TBG are highly sensitive to the “chiral ratio” κ , the physical value of which is not known precisely. Quoted ranges correspond to κ between 0.6 and 0.8, with the exception of Δ and W for uncorrected TBG, which was instead computed from a first-principles model of lattice relaxation [67]. The third column lists an extremely coarse estimate of the Coulomb interaction scale for the sake of comparison with Δ and W , given by $U_c \sim e^2/4\pi\epsilon L$ with $\epsilon/\epsilon_0 \sim 10$.

near band closings. We therefore refer to this region as the “optimal line.” In comparison, W and \bar{T} are both relatively uniform over most of the region, but tend to gradually decrease as V_{SL} becomes more negative. We thus conclude that the optimal parameters for realizing an FCI ground state in this phase, as indicated by single-particle energetics and band geometry, will likely lie near

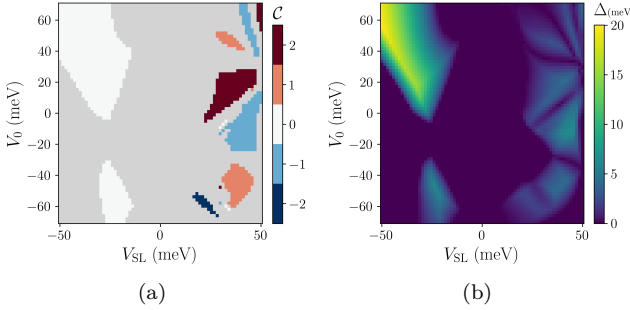


FIG. 6. (a) Chern number C and (b) band gap Δ of the $n = 1$ band of $L = 30$ nm triangular sBLG. Grayed regions of (a) indicated that the Chern number is not numerically well-resolved due to the proximity of a band closing.

the lower part of the optimal line. For example, at $(V_{SL}, V_0) = (30 \text{ meV}, -30 \text{ meV})$ (the same parameters used for Fig. 2, also indicated by a red star in Fig. 4), we find $\Delta = 10.3 \text{ meV}$, $W = 4.5 \text{ meV}$, $\bar{T} = 3.8$, and $F = 0.63$. This is tabulated in Fig. 5 together with estimates for the same indicators in magic angle TBG and twisted MoTe₂ for comparison. Since the energetic indicators Δ and W should rightfully be compared against the Coulomb interaction scale U_c , which is expected to differ between these systems due to their different superlattice periodicities, a crude estimate of $U_c \sim e^2/4\pi\epsilon L$ is also included in the table.

We finally remark that descending further below the optimal line (i.e. making V_0 more negative) can lead to modest improvements in W and \bar{T} at the cost of more significant penalties in Δ and F . For example, at $(V_{SL}, V_0) = (30 \text{ meV}, -45 \text{ meV})$, the indicator values are $\Delta = 6.6 \text{ meV}$, $W = 3.3 \text{ meV}$, $\bar{T} = 3.3$, and $F = 0.93$. Whether this turns out to be more favorable overall for realizing the FCI depends on the relative significance of the indicators.

2. $n = 1$ band

C and Δ for the $n = 1$ band as functions of V_{SL} and V_0 are shown in Fig. 6. There are three relatively prominent topological phases, with $C = +2$, -1 , and $+1$, in descending order of the V_0 at which they appear. Of these, the $C = -1$ phase has the most favorable indicators, attaining optimal values of $\Delta = 5.9 \text{ meV}$, $W = 8.4 \text{ meV}$, $\bar{T} = 8.6$, and $F = 1.4$ at $(V_{SL}, V_0) = (43 \text{ meV}, -11 \text{ meV})$. These are significantly worse than the optimal values found in the $n = 0$ band, so we conclude that the $n = 1$ band is not a good candidate in which to search for an FCI. However, we do remark that the $C = +2$ region exhibits the largest band gap ($\Delta = 4.3 \text{ meV}$) and range of parameter values of any $|C| > 1$ phase in a studied band and thus offers the most promising path to realizing higher-Chern physics in this system.

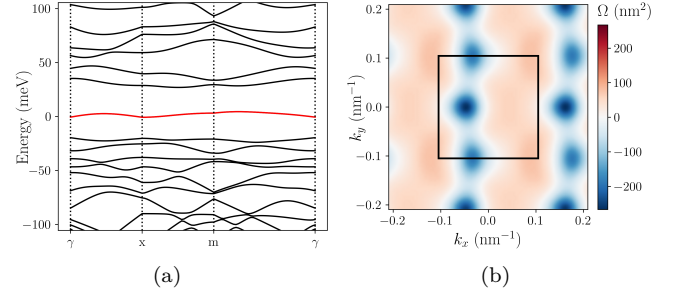


FIG. 7. (a) Band structure of square sBLG with $L = 30 \text{ nm}$, $V_{SL} = 30 \text{ meV}$, and $V_0 = 30 \text{ meV}$. The $n = 0$ band is highlighted. (b) Berry curvature distribution for the $n = 0$ band, which is topologically trivial. The boundary of the first superlattice Brillouin zone is overlaid in black.

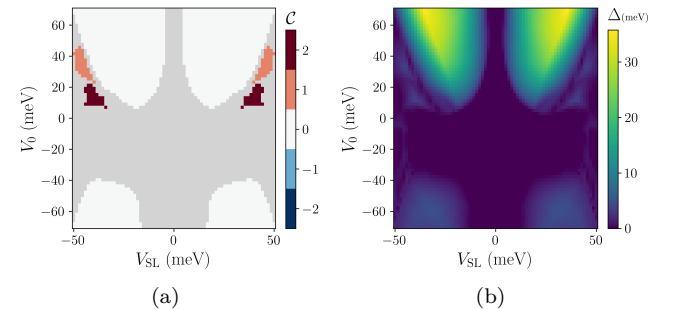


FIG. 8. (a) Chern number C and (b) band gap Δ of the $n = 0$ band of $L = 30$ nm square sBLG. Grayed regions of (a) indicated that the Chern number is not numerically well-resolved due to the proximity of a band closing.

3. $n < 0$ bands

There are flat bands with index $n < 0$ which can also become topological in certain parameter regimes. However, the phase diagrams of these bands are related to those of bands with $n \geq 0$ by a symmetry. If $v_4 = 0$ then H_{BLG} has an electron-hole symmetry generated by σ_z in the sublattice basis, i.e., σ_z anticommutes with \mathcal{H}_{BLG} . Since σ_z commutes with H_V , conjugation by σ_z together with an inversion of the parameters $(V_{SL}, V_0) \rightarrow (-V_{SL}, -V_0)$ leads to an overall inversion $H \rightarrow -H$. Thus, each $n < 0$ band is mapped by σ_z to an $n \geq 0$ band (specifically, $n \rightarrow -1 - n$) with a phase diagram that is identical upon inversion of V_{SL} and V_0 . Since v_4 is small, this correspondence is only slightly broken, so we will not comment further on the $n < 0$ bands.

B. Square superlattice

We also consider sBLG with a square superlattice geometry. The reciprocal lattice vectors are listed below Eq. (4). The band structure for this system is shown in Fig. 7(a) at example parameter values $(V_{SL}, V_0) =$

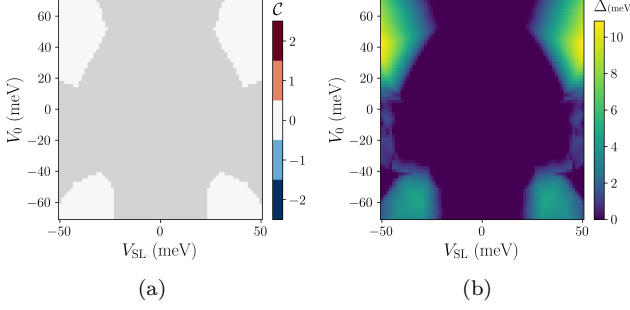


FIG. 9. (a) Chern number \mathcal{C} and (b) band gap Δ of the $n = 1$ band of $L = 30$ nm square sBLG. Grayed regions of (a) indicated that the Chern number is not numerically well-resolved due to the proximity of a band closing.

(30 meV, 30 meV). The $n = 0$ band, which in this case is not topological, is highlighted in red, and its Berry curvature distribution is shown in Fig. 7(b). Note that the four-fold rotational symmetry of the superlattice is broken by the trigonal warping of the underlying bilayer graphene dispersion. For $v_3 = 0$, the symmetry is restored.

\mathcal{C} and Δ as functions of V_{SL} and V_0 are shown for the $n = 0$ and $n = 1$ bands in Fig. 8 and Fig. 9, respectively. Note the symmetry of this phase diagram under a reflection $V_{\text{SL}} \rightarrow -V_{\text{SL}}$. This is a consequence of the fact that, for a square superlattice, translation in real space by $(L/2, L/2)$ corresponds to an inversion of the superlattice potential, but leaves both H_{BLG} and the uniform displacement potential V_0 unchanged.

Up to this symmetry, the $n = 0$ band has two topological phases in the scanned region of parameter space, with $\mathcal{C} = +1$ and $\mathcal{C} = +2$. However, both require fine-tuning of (V_{SL}, V_0) to access this small parameter regime and do not have band gaps exceeding 3.5 meV. Thus, we do not consider these regimes to be fruitful regions of phase space in which to search for an FCI. The $n = 1$ band, meanwhile, has no topological phases with $\Delta > 1.5$ meV at all in the scanned region, as shown in Fig. 9.

Based on these results, we conclude that square superlattice geometries are less favorable than triangular geometries for realizing topological flat bands in sBLG.

V. DEPENDENCE ON SUPERLATTICE PERIODICITY

We now consider the effect of rescaling the superlattice constant $L \rightarrow aL$. This rescales the Brillouin zone by $\mathbf{k} \rightarrow \mathbf{k}/a$, and thus Eq. (2) shows that simultaneously rescaling $t \rightarrow t/a$ rescales the entire effective Hamiltonian for BLG as $H_{\text{BLG}} \rightarrow H_{\text{BLG}}/a$. In other words, changing L is equivalent to an overall change of the energy scale of the system together with a renormalization of the interlayer hopping t , as one would predict from

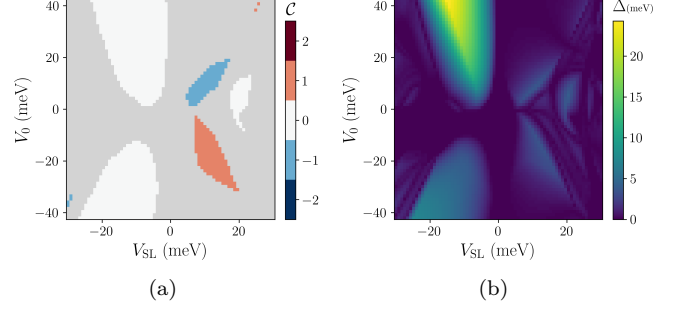


FIG. 10. (a) Chern number \mathcal{C} and (b) band gap Δ of the $n = 0$ band of $L = 50$ nm triangular sBLG. Grayed regions of (a) indicated that the Chern number is not numerically well-resolved due to the proximity of a band closing.

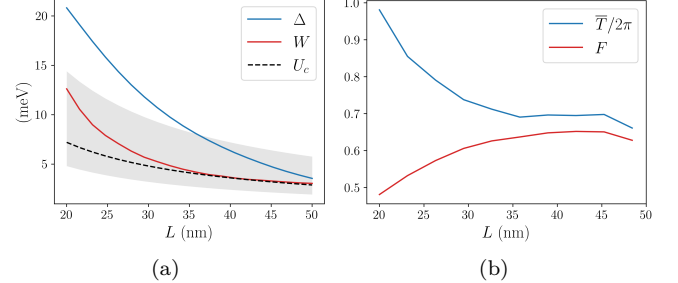


FIG. 11. Indicators as a function of L in triangular sBLG, with V_{SL} and V_0 chosen to maximize Δ within the $\mathcal{C} = +1$ phase of interest highlighted in Fig. 3. (a) Δ and W , together with an estimate of the Coulomb interaction scale $U_c \sim e^2/4\pi\epsilon L$. The dashed black line corresponds to $\epsilon/\epsilon_0 = 10$ while the shaded gray region corresponds to values between 5 and 15. (b) Quantum geometry indicators \bar{T} (divided by 2π to fit on a shared axis) and F .

dimensional analysis. This means that we generically expect larger values of L to lead to smaller band widths and gaps, and require lesser gate voltages to reach the regions of interest in the phase diagram. The renormalization of t does not substantially change this qualitative picture (compare Fig. 10, showing \mathcal{C} and Δ for the $n = 0$ band of $L = 50$ nm triangular sBLG, and Fig. 3, which shows the same for $L = 30$ nm), but it does have quantitative effects.

The band gap and bandwidth Δ and W are shown as functions of L in the prominent $\mathcal{C} = +1$ phase of triangular sBLG in Fig. 11(a). Since, as we showed in the previous section, Δ is the most sensitive indicator in this region and the other indicators tend to be reasonably well optimized near its maximum (see Fig. 4), the parameters V_{SL} and V_0 are selected at each value of L to maximize Δ . Also shown in Fig. 11(a) is an estimate of the Coulomb interaction scale $U_c \sim e^2/4\pi\epsilon L$. The dashed black line corresponds to $\epsilon/\epsilon_0 = 10$, the same value used in Fig. 5, while the shaded gray region corresponds to values between 5 and 15. Both Δ and W decrease with

L faster than the $1/L$ dependence predicted by naive dimensional analysis, and thus also faster than U_c , due to the renormalization of t . On the other hand, the relative band flatness Δ/W is maximized near $L = 30$ nm and quickly decreases for both larger and smaller L .

The quantum geometry indicators \bar{T} and F are shown in Fig. 11(b) as functions of L , using the same prescription for V_{SL} and V_0 as above. Neither of the quantum geometry markers vary significantly for L between 30 and 50 nm, but as L decreases below 30 nm, \bar{T} trends upward while F trends downward.

VI. CONCLUSION

We calculated the band structure and momentum-space quantum geometry of multiple bands near the Fermi level in both triangular and square sBLG across a wide range of parameter values. This allowed us to evaluate single-particle indicators for FCI stability and identify the most promising regions of the phase diagram for the experimental realization of an FCI. Our main result is that the most prominent topological phases appear in the $n = 0$ band of triangular sBLG, and that these phases exhibit an optimal line in parameter space along which the band gap is sharply maximized and other indicators remain favorable. At a superlattice length scale of $L = 30$ nm, this line extends from approximately $(V_{\text{SL}}, V_0) = (20 \text{ meV}, -12 \text{ meV})$ to $(35 \text{ meV}, -35 \text{ meV})$, with the most optimal values being near $(30 \text{ meV}, -30 \text{ meV})$, at which the single-particle indicators for FCI stability are similar to or

better than those for magic-angle TBG. Smaller values of L lead to greater band dispersion relative to the strength of the Coulomb interaction as well as less ideal quantum geometry, though band gaps increase and Berry curvature fluctuations decrease. Larger values lead to flatter bands and allow the phases of interest to be accessed with smaller applied gate voltages, but also result in substantially smaller band gaps.

Our results guide the experimental search for an FCI in sBLG. This guide can be expanded in future work by incorporating the effects of higher harmonics of the superlattice potential and considering non-Bravais superlattice geometries such as the kagome lattice. In addition, our analysis can be extended to other multilayer graphene stacks that realize topological flat bands [69].

ACKNOWLEDGMENTS

The authors thank Xu Du and Daniel Parker for useful conversations and correspondence. D.A., M.L., and A.D. acknowledge support from the National Science Foundation under the Columbia MRSEC on Precision-Assembled Quantum Materials (PAQM), Grant No. DMR-2011738. A.D. acknowledges support from the Keele and Jane and Aatos Erkko foundations as part of the SuperC collaboration. S.A.A.G. acknowledges support from the Air Force Office of Scientific Research under Grant No. FA9550-20-1-0260. In addition, J.C. acknowledges support from the Alfred P. Sloan Foundation through a Sloan Research Fellowship and from the Flatiron Institute, a division of the Simons Foundation.

-
- [1] R. Bistritzer and A. H. MacDonald, Moiré bands in twisted double-layer graphene, *Proceedings of the National Academy of Sciences* **108**, 12233 (2011).
 - [2] E. Suárez Morell, J. D. Correa, P. Vargas, M. Pacheco, and Z. Barticevic, Flat bands in slightly twisted bilayer graphene: Tight-binding calculations, *Phys. Rev. B* **82**, 121407 (2010).
 - [3] Y. Cao, V. Fatemi, A. Demir, S. Fang, S. L. Tomarken, J. Y. Luo, J. D. Sanchez-Yamagishi, K. Watanabe, T. Taniguchi, E. Kaxiras, *et al.*, Correlated insulator behaviour at half-filling in magic-angle graphene superlattices, *Nature* **556**, 80 (2018).
 - [4] Y. Cao, V. Fatemi, S. Fang, K. Watanabe, T. Taniguchi, E. Kaxiras, and P. Jarillo-Herrero, Unconventional superconductivity in magic-angle graphene superlattices, *Nature* **556**, 43 (2018).
 - [5] G. Tarnopolsky, A. J. Kruchkov, and A. Vishwanath, Origin of magic angles in twisted bilayer graphene, *Phys. Rev. Lett.* **122**, 106405 (2019).
 - [6] F. Wu, T. Lovorn, E. Tutuc, I. Martin, and A. MacDonald, Topological insulators in twisted transition metal dichalcogenide homobilayers, *Physical review letters* **122**, 086402 (2019).
 - [7] H. Pan, F. Wu, and S. Das Sarma, Band topology, Hubbard model, Heisenberg model, and Dzyaloshinskii-Moriya interaction in twisted bilayer WSe₂, *Physical Review Research* **2**, 033087 (2020).
 - [8] T. Devakul, V. Crépel, Y. Zhang, and L. Fu, Magic in twisted transition metal dichalcogenide bilayers, *Nature communications* **12**, 6730 (2021).
 - [9] H. Pan, M. Xie, F. Wu, and S. Das Sarma, Topological phases in AB-stacked MoTe₂/WSe₂: z_2 topological insulators, Chern insulators, and topological charge density waves, *Physical Review Letters* **129**, 056804 (2022).
 - [10] Y. Zhang, T. Devakul, and L. Fu, Spin-textured Chern bands in AB-stacked transition metal dichalcogenide bilayers, *Proceedings of the National Academy of Sciences* **118**, e2112673118 (2021).
 - [11] V. Crépel and J. Cano, Efficient prediction of superlattice and anomalous miniband topology from quantum geometry, *Physical Review X* **15**, 011004 (2025).
 - [12] M. Serlin, C. Tschirhart, H. Polshyn, Y. Zhang, J. Zhu, K. Watanabe, T. Taniguchi, L. Balents, and A. Young, Intrinsic quantized anomalous Hall effect in a moiré heterostructure, *Science* **367**, 900 (2020).

- [13] A. L. Sharpe, E. J. Fox, A. W. Barnard, J. Finney, K. Watanabe, T. Taniguchi, M. Kastner, and D. Goldhaber-Gordon, Emergent ferromagnetism near three-quarters filling in twisted bilayer graphene, *Science* **365**, 605 (2019).
- [14] T. Li, S. Jiang, B. Shen, Y. Zhang, L. Li, Z. Tao, T. Devakul, K. Watanabe, T. Taniguchi, L. Fu, J. Shan, and K. F. Mak, Quantum anomalous hall effect from intertwined moirébands, *Nature* **600**, 641 (2021).
- [15] K. P. Nuckolls, M. Oh, D. Wong, B. Lian, K. Watanabe, T. Taniguchi, B. A. Bernevig, and A. Yazdani, Strongly correlated chern insulators in magic-angle twisted bilayer graphene, *Nature* **588**, 610 (2020).
- [16] Y. Xie, A. T. Pierce, J. M. Park, D. E. Parker, E. Khalaf, P. Ledwith, Y. Cao, S. H. Lee, S. Chen, P. R. Forrester, K. Watanabe, T. Taniguchi, A. Vishwanath, P. Jarillo-Herrero, and A. Yacoby, Fractional chern insulators in magic-angle twisted bilayer graphene, *Nature* **600**, 439 (2021).
- [17] C. R. Dean, L. Wang, P. Maher, C. Forsythe, F. Ghahari, Y. Gao, J. Katoch, M. Ishigami, P. Moon, M. Koshino, T. Taniguchi, K. Watanabe, K. L. Shepard, J. Hone, and P. Kim, Hofstadter's butterfly and the fractal quantum hall effect in moirésuperlattices, *Nature* **497**, 598 (2013).
- [18] B. Hunt, J. D. Sanchez-Yamagishi, A. F. Young, M. Yankowitz, B. J. LeRoy, K. Watanabe, T. Taniguchi, P. Moon, M. Koshino, P. Jarillo-Herrero, and R. C. Ashoori, Massive dirac fermions and hofstadter butterfly in a van der waals heterostructure, *Science* **340**, 1427 (2013), <https://www.science.org/doi/pdf/10.1126/science.1237240>.
- [19] L. A. Ponomarenko, R. V. Gorbachev, G. L. Yu, D. C. Elias, R. Jalil, A. A. Patel, A. Mishchenko, A. S. Mayorov, C. R. Woods, J. R. Wallbank, M. Mucha-Kruczynski, B. A. Piot, M. Potemski, I. V. Grigorieva, K. S. Novoselov, F. Guinea, V. I. Fal'ko, and A. K. Geim, Cloning of dirac fermions in graphene superlattices, *Nature* **497**, 594 (2013).
- [20] E. M. Spanton, A. A. Zibrov, H. Zhou, T. Taniguchi, K. Watanabe, M. P. Zaletel, and A. F. Young, Observation of fractional chern insulators in a van der waals heterostructure, *Science* **360**, 62 (2018), <https://www.science.org/doi/pdf/10.1126/science.aan8458>.
- [21] N. Regnault and B. A. Bernevig, Fractional chern insulator, *Phys. Rev. X* **1**, 021014 (2011).
- [22] D. Sheng, Z.-C. Gu, K. Sun, and L. Sheng, Fractional quantum Hall effect in the absence of Landau levels, *Nature communications* **2**, 389 (2011).
- [23] T. Neupert, L. Santos, C. Chamon, and C. Mudry, Fractional quantum Hall states at zero magnetic field, *Physical review letters* **106**, 236804 (2011).
- [24] J. Cai, E. Anderson, C. Wang, X. Zhang, X. Liu, W. Holtzmann, Y. Zhang, F. Fan, T. Taniguchi, K. Watanabe, Y. Ran, T. Cao, L. Fu, D. Xiao, W. Yao, and X. Xu, Signatures of fractional quantum anomalous Hall states in twisted MoTe₂, *Nature* **622**, 63 (2023).
- [25] H. Park, J. Cai, E. Anderson, Y. Zhang, J. Zhu, X. Liu, C. Wang, W. Holtzmann, C. Hu, Z. Liu, T. Taniguchi, K. Watanabe, J.-H. Chu, T. Cao, L. Fu, W. Yao, C.-Z. Chang, D. Cobden, D. Xiao, and X. Xu, Observation of fractionally quantized anomalous Hall effect, *Nature* **622**, 74 (2023).
- [26] Y. Zeng, Z. Xia, K. Kang, J. Zhu, P. Knüppel, C. Vaswani, K. Watanabe, T. Taniguchi, K. F. Mak, and J. Shan, Thermodynamic evidence of fractional chern insulator in moiréband2, *Nature* **622**, 69 (2023).
- [27] Z. Lu, T. Han, Y. Yao, A. P. Reddy, J. Yang, J. Seo, K. Watanabe, T. Taniguchi, L. Fu, and L. Ju, Fractional quantum anomalous hall effect in multilayer graphene, *Nature* **626**, 759 (2024).
- [28] J. Xie, Z. Huo, X. Lu, Z. Feng, Z. Zhang, W. Wang, Q. Yang, K. Watanabe, T. Taniguchi, K. Liu, Z. Song, X. C. Xie, J. Liu, and X. Lu, Tunable fractional chern insulators in rhombohedral graphene superlattices, *Nature Materials* **10.1038/s41563-025-02225-7** (2025).
- [29] C. Forsythe, X. Zhou, K. Watanabe, T. Taniguchi, A. Pasupathy, P. Moon, M. Koshino, P. Kim, and C. R. Dean, Band structure engineering of 2d materials using patterned dielectric superlattices, *Nature nanotechnology* **13**, 566 (2018).
- [30] S. Wang, D. Scarabelli, L. Du, Y. Y. Kuznetsova, L. N. Pfeiffer, K. W. West, G. C. Gardner, M. J. Manfra, V. Pellegrini, S. J. Wind, *et al.*, Observation of Dirac bands in artificial graphene in small-period nanopatterned GaAs quantum wells, *Nature nanotechnology* **13**, 29 (2018).
- [31] Y. Li, S. Dietrich, C. Forsythe, T. Taniguchi, K. Watanabe, P. Moon, and C. R. Dean, Anisotropic band flattening in graphene with one-dimensional superlattices, *Nature Nanotechnology* **16**, 525 (2021).
- [32] D. Barcons Ruiz, H. Herzig Sheinfux, R. Hoffmann, I. Torre, H. Agarwal, R. K. Kumar, L. Vistoli, T. Taniguchi, K. Watanabe, A. Bachtold, and F. H. L. Koppens, Engineering high quality graphene superlattices via ion milled ultra-thin etching masks, *Nature Communications* **13**, 6926 (2022).
- [33] D. Q. Wang, Z. Krix, O. P. Sushkov, I. Farrer, D. A. Ritchie, A. R. Hamilton, and O. Klochan, Formation of artificial fermi surfaces with a triangular superlattice on a conventional two-dimensional electron gas, *Nano Letters* **23**, 1705 (2023).
- [34] J. Sun, S. A. Akbar Ghorashi, K. Watanabe, T. Taniguchi, F. Camino, J. Cano, and X. Du, Signature of correlated insulator in electric field controlled superlattice, *Nano Letters* **24**, 13600 (2024), pMID: 39432385, <https://doi.org/10.1021/acs.nanolett.4c03238>.
- [35] D. Q. Wang, Z. Krix, O. A. Tkachenko, V. A. Tkachenko, C. Chen, I. Farrer, D. A. Ritchie, O. P. Sushkov, A. R. Hamilton, and O. Klochan, Tuning the bandstructure of electrons in a two-dimensional artificial electrostatic crystal in GaAs quantum wells, arXiv preprint arXiv:2402.12769 (2024).
- [36] K. Yasuda, X. Wang, K. Watanabe, T. Taniguchi, and P. Jarillo-Herrero, Stacking-engineered ferroelectricity in bilayer boron nitride, *Science* **372**, 1458 (2021).
- [37] M. Vizner Stern, Y. Waschitz, W. Cao, I. Nevo, K. Watanabe, T. Taniguchi, E. Sela, M. Urbakh, O. Hod, and M. Ben Shalom, Interfacial ferroelectricity by van der waals sliding, *Science* **372**, 1462 (2021).
- [38] X. Wang, K. Yasuda, Y. Zhang, S. Liu, K. Watanabe, T. Taniguchi, J. Hone, L. Fu, and P. Jarillo-Herrero, Interfacial ferroelectricity in rhombohedral-stacked bilayer transition metal dichalcogenides, *Nature nanotechnology* **17**, 367 (2022).
- [39] D. S. Kim, R. C. Dominguez, R. Mayorga-Luna, D. Ye, J. Embley, T. Tan, Y. Ni, Z. Liu, M. Ford, F. Y. Gao, *et al.*, Electrostatic moiré potential from twisted hexagonal boron nitride layers, *Nature materials* **23**, 65

- (2024).
- [40] Z. Zhang, J. Xie, W. Zhao, R. Qi, C. Sanborn, S. Wang, S. Kahn, K. Watanabe, T. Taniguchi, A. Zettl, *et al.*, Engineering correlated insulators in bilayer graphene with a remote Coulomb superlattice, *Nature Materials* **23**, 189 (2024).
- [41] X. Wang, C. Xu, S. Aronson, D. Bennett, N. Paul, P. J. Crowley, C. Collignon, K. Watanabe, T. Taniguchi, R. Ashoori, *et al.*, Moiré band structure engineering using a twisted boron nitride substrate, *Nature Communications* **16**, 178 (2025).
- [42] K. K. Gomes, W. Mar, W. Ko, F. Guinea, and H. C. Manoharan, Designer dirac fermions and topological phases in molecular graphene, *Nature* **483**, 306 (2012).
- [43] L.-k. Shi, J. Ma, and J. C. Song, Gate-tunable flat bands in van der waals patterned dielectric superlattices, *2D Materials* **7**, 015028 (2019).
- [44] S. A. A. Ghorashi, A. Dunbrack, A. Abouelkomansan, J. Sun, X. Du, and J. Cano, Topological and stacked flat bands in bilayer graphene with a superlattice potential, *Phys. Rev. Lett.* **130**, 196201 (2023).
- [45] Z. Krix and O. P. Sushkov, Patterned bilayer graphene as a tunable strongly correlated system, *Physical Review B* **107**, 165158 (2023).
- [46] V. Crépel, A. Dunbrack, D. Guerci, J. Bonini, and J. Cano, Chiral model of twisted bilayer graphene realized in a monolayer, *Physical Review B* **108**, 075126 (2023).
- [47] Q. Gao, J. Dong, P. Ledwith, D. Parker, and E. Khalaf, Untwisting moiré physics: Almost ideal bands and fractional chern insulators in periodically strained monolayer graphene, *Phys. Rev. Lett.* **131**, 096401 (2023).
- [48] X. Wan, S. Sarkar, S.-Z. Lin, and K. Sun, Topological exact flat bands in two-dimensional materials under periodic strain, *Physical Review Letters* **130**, 216401 (2023).
- [49] Y. Zeng, T. M. Wolf, C. Huang, N. Wei, S. A. A. Ghorashi, A. H. MacDonald, and J. Cano, Gate-tunable topological phases in superlattice modulated bilayer graphene, *Physical Review B* **109**, 195406 (2024).
- [50] C. N. Lau, M. W. Bockrath, K. F. Mak, and F. Zhang, Reproducibility in the fabrication and physics of moiré materials, *Nature* **602**, 41 (2022).
- [51] E. McCann and M. Koshino, The electronic properties of bilayer graphene, *Reports on Progress in physics* **76**, 056503 (2013).
- [52] A. B. Kuzmenko, I. Crassee, D. van der Marel, P. Blake, and K. S. Novoselov, Determination of the gate-tunable band gap and tight-binding parameters in bilayer graphene using infrared spectroscopy, *Phys. Rev. B* **80**, 165406 (2009).
- [53] H. Rokni and W. Lu, Layer-by-layer insight into electrostatic charge distribution of few-layer graphene, *Scientific reports* **7**, 42821 (2017).
- [54] S. A. Parameswaran, R. Roy, and S. L. Sondhi, Fractional chern insulators and the W_∞ algebra, *Phys. Rev. B* **85**, 241308 (2012).
- [55] R. Roy, Band geometry of fractional topological insulators, *Phys. Rev. B* **90**, 165139 (2014).
- [56] M. Claassen, C. H. Lee, R. Thomale, X.-L. Qi, and T. P. Devereaux, Position-momentum duality and fractional quantum hall effect in chern insulators, *Physical review letters* **114**, 236802 (2015).
- [57] T. S. Jackson, G. Möller, and R. Roy, Geometric stability of topological lattice phases, *Nature communications* **6**, 8629 (2015).
- [58] D. Bauer, T. Jackson, and R. Roy, Quantum geometry and stability of the fractional quantum hall effect in the hofstadter model, *Physical Review B* **93**, 235133 (2016).
- [59] P. J. Ledwith, G. Tarnopolsky, E. Khalaf, and A. Vishwanath, Fractional chern insulator states in twisted bilayer graphene: An analytical approach, *Phys. Rev. Res.* **2**, 023237 (2020).
- [60] J. Wang, J. Cano, A. J. Millis, Z. Liu, and B. Yang, Exact landau level description of geometry and interaction in a flatband, *Phys. Rev. Lett.* **127**, 246403 (2021).
- [61] B. Mera and T. Ozawa, Kähler geometry and chern insulators: Relations between topology and the quantum metric, *Physical Review B* **104**, 045104 (2021).
- [62] B. Estienne, N. Regnault, and V. Crépel, Ideal chern bands as landau levels in curved space, *Phys. Rev. Res.* **5**, L032048 (2023).
- [63] P. J. Ledwith, A. Vishwanath, and D. E. Parker, Vortexability: A unifying criterion for ideal fractional chern insulators, *Physical Review B* **108**, 205144 (2023).
- [64] N. Morales-Durán, J. Wang, G. R. Schleider, M. Angeli, Z. Zhu, E. Kaxiras, C. Repellin, and J. Cano, Pressure-enhanced fractional chern insulators along a magic line in moiré transition metal dichalcogenides, *Physical Review Research* **5**, L032022 (2023).
- [65] S. H. Simon and M. S. Rudner, Contrasting lattice geometry dependent versus independent quantities: Ramifications for berry curvature, energy gaps, and dynamics, *Physical Review B* **102**, 165148 (2020).
- [66] D. Parker, P. Ledwith, E. Khalaf, T. Soejima, J. Hauschild, Y. Xie, A. Pierce, M. P. Zaletel, A. Yacoby, and A. Vishwanath, Field-tuned and zero-field fractional chern insulators in magic angle graphene, arXiv preprint arXiv:2112.13837 (2021).
- [67] N. N. T. Nam and M. Koshino, Lattice relaxation and energy band modulation in twisted bilayer graphene, *Phys. Rev. B* **96**, 075311 (2017).
- [68] J. Dong, J. Wang, P. J. Ledwith, A. Vishwanath, and D. E. Parker, Composite fermi liquid at zero magnetic field in twisted mote₂, *Phys. Rev. Lett.* **131**, 136502 (2023).
- [69] S. A. A. Ghorashi and J. Cano, Multilayer graphene with a superlattice potential, *Phys. Rev. B* **107**, 195423 (2023).